Temperatures, polar mesosphere summer echoes, and noctilucent clouds over Spitsbergen (78°N)

Franz-Josef Lübken, Marius Zecha, and Josef Höffner
Leibniz-Institute of Atmospheric Physics, Kühlungsborn, Germany

Jürgen Röttger
Max Planck Institute for Aeronomy, Katlenburg-Lindau, Germany

Received 14 October 2003; revised 3 March 2004; accepted 22 March 2004; published 12 June 2004.

[1] Simultaneous measurements of temperatures, polar mesosphere summer echoes (PMSE), and noctilucent clouds (NLC) took place in the polar cap (78°N) during the Rocketborne Observations in the Middle Atmosphere campaign (ROMA) in summer 2001. PMSE were observed practically permanently from the beginning and prior to the ROMA campaign (mid-July) until mid-August and disappeared by the end of August. PMSE occur between 81 and 92 km but have maximum occurrence rates between 83 and 89 km (up to 80% per day). PMSE are compared with temperatures from falling spheres, with frost point temperatures (T_f), and with degrees of saturation (S) using water vapor mixing ratios from models. PMSE occur nearly exclusively at altitudes with supersaturation, but the reverse is not true. Temperatures within PMSE layers can be up to 20–25 K below T_f. There is no correlation between the radar echo power and the magnitude of S. Around the mesopause we frequently find S values significantly larger than 1 (up to 13000) at altitudes with the confirmed absence of PMSE. This could indicate that the actual water vapor mixing ratio is substantially smaller than our assumed model values in line with the "freeze-drying effect." The mean of all NLC peak altitudes is 83.6 km (variability: ±1.1 km), and the occurrence rate is 77% in the main summer season. Most of the time the lower edges of PMSE and NLC are colocated within a few hundred meters or less, which can be explained by a rapid evaporation of ice particles. This close agreement also indicates a rather homogeneous horizontal distribution of ice particles at scales below a few kilometers. The seasonal and height variation of PMSE nicely agrees with the time/height range of S > 1 and confirms the overwhelming importance of low enough temperatures for the existence of PMSE. The variation of NLC also agrees with the seasonal variation of S but covers only the lower height range with supersaturation in line with the different sensitivity of NLC and PMSE on particle radius. From the combined observations of PMSE and NLC, mean occurrence rates of neutral air turbulence of larger than ~50% are deduced. The experimental results at Spitsbergen confirm the standard scenario of PMSE and NLC, namely that particles start to nucleate around the mesopause, and grow and sediment until they reach "warm" atmospheric regions around 82 km where they quickly evaporate. Small ice particles can affect the plasma leading to PMSE, whereas they need to grow to radii larger than approximately 20 nm to be seen by lidar. *INDEX TERMS:* 0305 Atmospheric Composition and Structure: Aerosols and particles (0345, 4801); 0340 Atmospheric Composition and Structure: Middle atmosphere—composition and chemistry; 2439 Ionosphere: Ionospheric irregularities; 2475 Ionosphere: Polar cap ionosphere; *KEYWORDS:* temperature, PMSE, NLC

Citation: Lübken, F.-J., M. Zecha, J. Höffner, and J. Röttger (2004), Temperatures, polar mesosphere summer echoes, and noctilucent clouds over Spitsbergen (78°N), *J. Geophys. Res.*, *109*, D11203, doi:10.1029/2003JD004247.

1. Introduction

[2] Remote sensing of layers in the upper mesosphere can provide important information about the thermal and dynamical background conditions in a section of our atmosphere which is experimentally difficult to access. Important examples of such layers are "polar mesosphere summer echoes" (PMSE), and "noctilucent clouds" (NLC). As will be explained later, both phenomena are related to ice particles which can only exist if temperatures are below ~130–150 K. The common measurement of temperatures,

0148-0227/04/2003JD004247$09.00

PMSE, and NLC therefore helps to better understand the relationship between the thermal structure of the mesopause region and the existence of ice particles. This can be very helpful at other places where NLC/PMSE are detected but no temperature measurements are available.

[3] PMSE are very strong radar signals received from the summer mesopause region at polar and, to a lesser extent, also at midlatitudes. On the basis of some key ideas and observations presented earlier a comprehensive understanding of the physical processes leading to PMSE has been developed only recently [*Kelley et al.*, 1987; *Cho et al.*, 1992; *Lübken et al.*, 1993; *Röttger*, 1994; *Cho and Röttger*, 1997; *Hill et al.*, 1999; *Lie-Svendson et al.*, 2003; *Blix et al.*, 2003; *Rapp and Lübken*, 2003]. We concentrate on VHF radars with a typical wavelength of λ = 6 m where scattering requires the presence of meter-scale structures in the electron gas. These structures are created by neutral turbulence mixing the electron gas. Owing to the diffusivity reduction of the electrons in the presence of "heavy" charged ice particles the structures in the electron gas extend beyond the neutral turbulence convective subrange to the short Bragg scale (3 m) of the radar [see, e.g., *Lübken et al.*, 2002, and references therein]. The reduced diffusivity allows spatial variations in the plasma at scales smaller than the smallest scales in the neutral gas. Roughly speaking the PMSE signal is proportional to $N_A r_A^2$ where N_A is the number of ice particles, and r_A is their radius [*Rapp et al.*, 2003]. The apparent noncorrelation of PMSE and neutral turbulence occasionally observed with simultaneous radar and in situ measurements is explained by the slow decay of plasma irregularities after neutral turbulence has ceased. The time constant for this decay is proportional to r_A^2 and reaches 1.5 hours for r_A = 30 nm [*Lübken et al.*, 2002; *Rapp and Lübken*, 2003]. The current PMSE theory is in agreement with the mean characteristics of PMSE and with in situ observations of plasma irregularities and turbulence. The improved understanding of PMSE can now be used to learn more about the thermal and dynamical status of the background atmosphere. Most important, PMSE require the presence of ice particles and therefore supersaturation conditions, at least in the climatological sense.

[4] Noctilucent clouds exist of ice particles which are observed in the summer season at middle and polar latitudes by lidar or, if the observer is in the dark, by naked eye [*Gadsden and Schröder*, 1989; *Hansen et al.*, 1989; *von Cossart et al.*, 1999; *Thayer et al.*, 2003; *Fiedler et al.*, 2003]. The visibility of NLC both for the lidars and the human observer varies with r_A^6, i.e., whether or not a NLC is observed by optical instruments critically depends on the size of the particles. Roughly speaking a NLC can be detected if the particles are larger than ~20 nm, whereas particles can be as small as ~3 nm to create PMSE [*Rapp and Lübken*, 2003]. It is this different ice particle size dependence of NLC and PMSE in conjunction with the thermal structure which is important to understand the different seasonal and height variations presented later.

[5] In this paper we summarize simultaneous observations of temperatures, PMSE, and NLC performed in 2001 at very high latitudes (Longyearbyen, 78°N). After introducing the experimental techniques in section 2 we will compare the height and seasonal variation of PMSE and NLC with the corresponding variation of the thermal structure in section 3. The geophysical implications of these observations are discussed in section 4.

2. Experimental Techniques

2.1. Temperatures From Falling Spheres

[6] From 16 July to 14 September 2001, a series of small meteorological rockets were launched from a mobile launcher installed close to Longyearbyen (78°N, 15°E) on the north polar island Spitsbergen which is part of the archipelago Svalbard. The campaign was labeled "ROMA" (Rocketborne Observations in the Middle Atmosphere). The temperature measurements reported here were performed employing the "falling sphere" (FS) technique which is described in detail elsewhere [*Schmidlin*, 1991]. This technique gives densities and horizontal winds in an altitude range from approximately 95 to 30 km. Temperatures are obtained by integrating the density profile assuming hydrostatic equilibrium. The temperature at the top of the FS profile ("start temperature" $T_{\circ}$) has to be taken from independent measurements or from a model. We have taken $T_{\circ}$ from a preliminary data analysis of the potassium lidar measurements (described below) which gave interpolated and smoothed temperature profiles for the entire ROMA period (J. Höffner, private communication, 2003). The availability of lidar temperatures significantly improves the FS accuracy in the upper part of the profiles since it reduces the uncertainty about the start temperature. The height-dependent sphere reaction time constant causes a smoothing of the density, temperature, and wind profiles. The smallest scales detectable are typically 8, 3, and 0.8 km at 85, 60, and 40 km, respectively. The uncertainty of the temperatures is typically 7, 3, and 1.5 K at 90, 80, and 70 km. We note that the FS technique shows excellent overall agreement with entirely different rocketborne temperature measurements with much better altitude resolution [*Rapp et al.*, 2002b]. In particular the mean mesopause structure is nicely reproduced. Individual profiles, details on the launch sequence, and a temperature climatology are presented in the work of *Lübken and Müllemann* [2003].

2.2. SOUSY Svalbard Radar and IAP Potassium Lidar

[7] The SOUSY Svalbard Radar is an MST VHF radar installed by the Max-Planck-Institut für Aeronomie in 1998. It is operated routinely on campaign bases since summer 1999. Its original scientific aims and technical specifications are summarized by *Czechowsky et al.* [1998]. First results regarding the seasonal and height variation of PMSE at Spitsbergen are published by *Rüster et al.* [2001]. *Röttger* [2001] described the operational parameters and details of PMSE observations with the SOUSY Svalbard Radar and the EISCAT Svalbard Radar, which operates at 500 MHz, i.e., at a radar Bragg scale almost ten times larger than that of the SOUSY Svalbard Radar. A more detailed description of comparisons and a comprehensive summary of PMSE statistics from various seasons will be published in the near future.

[8] Noctilucent clouds and atmospheric temperatures are observed by the potassium lidar of the Leibniz-Institute of Atmospheric Physics in Kühlungsborn [*von Zahn and Höffner*, 1996]. This technique allows to

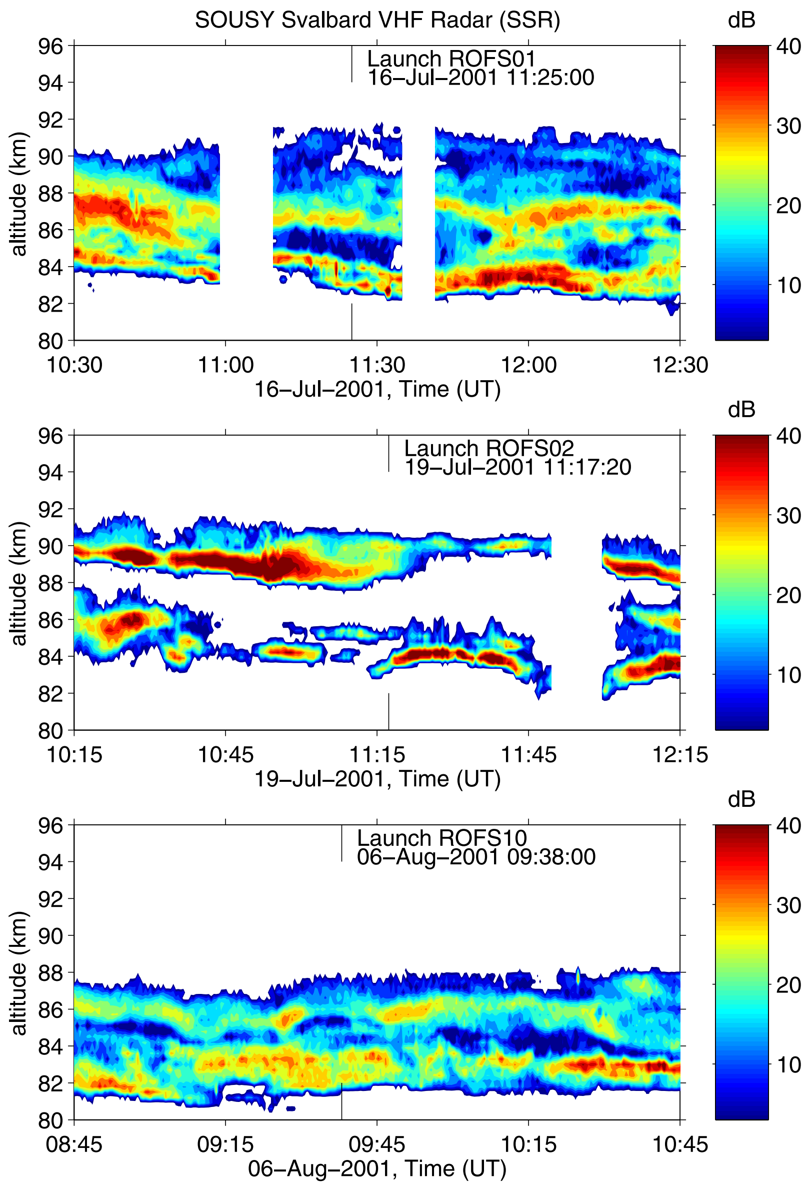

Figure 1. PMSE layers during flights (top) ROFS01, (middle) ROFS02, and (bottom) ROFS10. The color-coded contours show the signal above noise. Launch times are given and marked in the plots. Occasional gaps are caused by radar switch off by the local air traffic control, e.g., shortly before and after ROFS01.

deduce atmospheric temperatures in the potassium layer from measurements of the spectral width of the Doppler broadened K-D_1 resonance line at 769.9 nm, even during full daylight conditions [*Fricke-Begemann et al.*, 2002]. The lidar container was transported to Svalbard in May 2001 and observations were performed in the periods 12 June until 5 October 2001, 27 February until 24 March 2002, and 31 March until 21 August 2003, respectively. First results from these measurements including a comparison with FS temperature profiles are presented by J. Höffner et al. (private communication, 2004). In this paper we concentrate on the K lidar measurements of NLC during the ROMA campaign which are detected as an enhanced signal (relative to the background noise and the air molecule signal) which does not vary when the laser frequency is tuned over the potassium resonance line. More details and first results on NLC are published in the work of *Höffner et al.* [2003].

3. Results

3.1. PMSE Statistics

[9] In Figure 1 we show three examples of PMSE measured around the launches of FS flights ROFS01, ROFS02, and ROFS10, respectively. The launch dates and times are given in the plot. Very strong radar echoes up to 35 dB above noise level (corresponding to a radar reflectivity of about 10^{-14} m^{-1}) are present quasi permanently. There are some gaps in the time series (for example shortly before and after flight ROFS01) which are caused by a radar stand-by issued by the local air traffic control. PMSE appear approximately between 81 and 92 km and exhibit a large

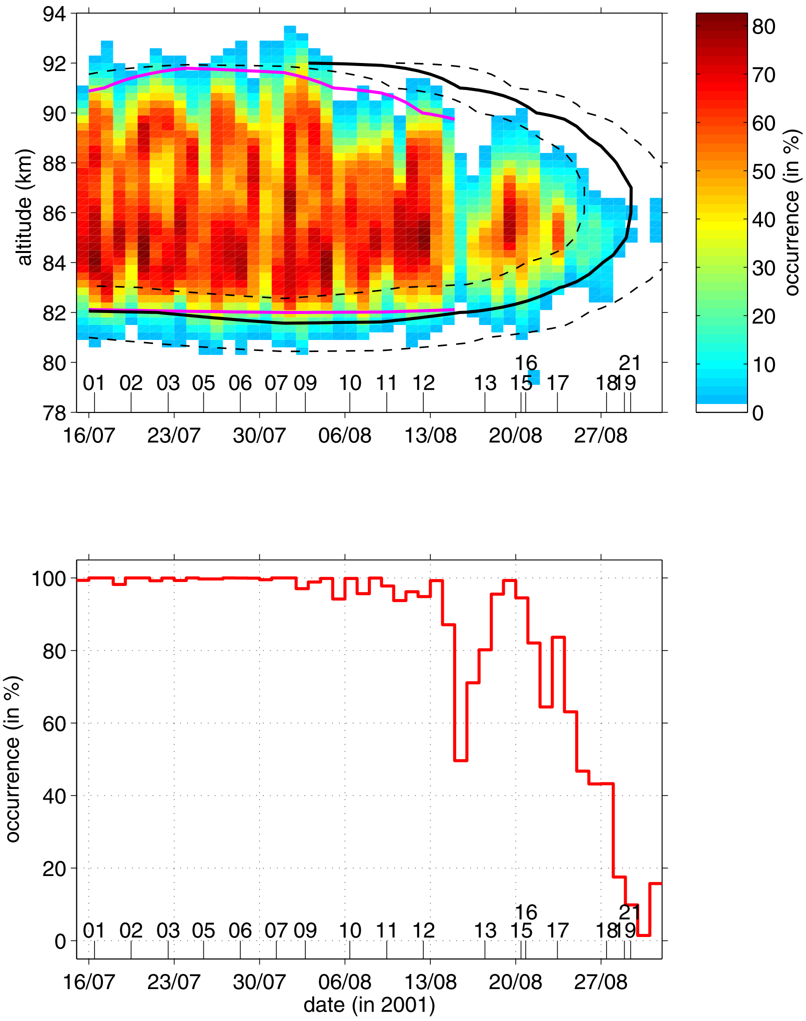

Figure 2. (top) Seasonal variation of the occurrence of PMSE. The occurrence rate averaged over 24 hours is shown as a function of season and altitude. We also show the S = 1 line using the falling sphere (FS) temperature climatology and model water vapor values from K&S (black line) and vZ&B (pink line), respectively (see text for more details). The black dashed lines show S = 1 lines with K&S water vapor values and FS temperatures varied by ±5 K. (bottom) Cumulative occurrence rate. For example, a value of 90% means that during that day a PMSE was detected at 90% of the time in at least one altitude. PMSE are present permanently until mid-August. There is a significant reduction in occurrence around 15 August for unknown reasons.

variety in their morphology. They can appear quasi homogeneously in altitude (top and bottom panels of Figure 1) but also in two or more distinct layers (middle panel of Figure 1).

[10] In Figure 2 the occurrence rate of PMSE averaged over 24 h is shown for all days from 15 July (beginning of ROMA campaign) until end of August. PMSE occur between approximately 81 and 92 km with typical daily occurrence rates of up to 60–80% in the center (~83–89 km) and very small rates at the edges. The transition is somewhat steeper at the lower PMSE edge compared to above. The altitude extent of PMSE is fairly uniform throughout the summer season and shrinks after approximately 20 August starting from the top heights. No more PMSE were observed after 31 August. A cumulative occurrence frequency is shown in the lower part of Figure 2. For example, a value of 90% means that during 90% of that day a PMSE was observed in at least one altitude. As can be seen from this figure PMSE are present practically all the time in the main summer season and disappear rather quickly (within 1–2 weeks) after 20 August. Of course, the occurrence of PMSE depends on the sensitivity of the radar, which means that this statement is true for the radar peak power-aperture product of about 5 × 10^8 Wm^2 for the SOUSY Svalbard Radar (see *Röttger* [2001] for detailed system parameters). For yet unknown geophysical reasons there is a marked decrease in PMSE occurrence frequency around 15 August. As will be discussed in detail later there is no apparent temperature increase in this period. The cumulative height distribution of PMSE occurrence rate is shown in Figure 3 where we have plotted the seasonal integrated time for a PMSE to occur in a certain altitude. The total time that measurements where made is 1096 hours which is 95% of the time from 15 July to 31 August (=1152 hours). This

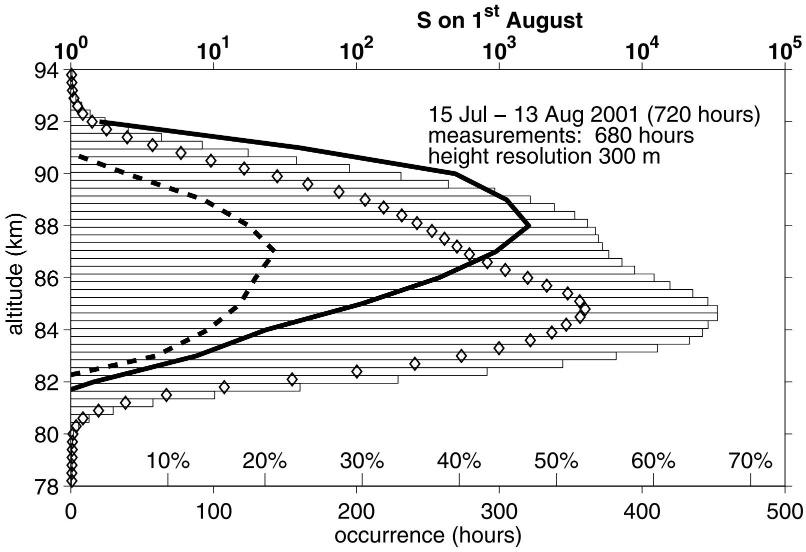

Figure 3. Height dependence of the occurrence rate of PMSE for the period 15 July to 13 August 2001. The maximum occurrence of PMSE is ~450 hours around 85 km, which corresponds to a rate of 66%. If we extend the time period to 31 August, we arrive at ~53% (diamonds) and 580 hours (caution: the lower axis for hours is only correct for the former time period, i.e., 15.7–31.8). The solid and dashed lines present the degree of saturation using temperatures from the falling sphere climatology and water vapor profiles for 1 August from the K&S and vZ&B models, respectively.

means that the radar was taking data practically permanently during the ROMA campaign. Concentrating on the mean season (15 July to 13 August) PMSE occur most frequent (up to more than 60%) in the center of the height region (~83–87 km) whereas they are quite rare (<10%) below 81 and above 91 km. The distribution shown in Figure 3 is not symmetric about the maximum but shows a "shoulder" at heights above the maximum. This is presumably a typical feature since it has been observed in other years [*Rüster et al.*, 2001].

3.2. Water Vapor Profile

[11] In the following sections we will present temperature measurements in the vicinity of PMSE and NLC which are most easily interpreted by studying the degree of saturation of water vapor, S, and the frost point temperature, T_f. The degree of saturation is defined as $S = p_{H_2O}/p_{sat}$, where p_{H_2O} is the partial pressure of water vapor, and p_{sat} is the saturation pressure of water vapor over ice [*Mauersberger and Krankowsky*, 2003]. If $S > 1$ particles can exist or grow, and if $S < 1$ they will evaporate. p_{sat} varies exponentially with temperature, i.e., S is critically dependent on temperature and to a lesser extent on the water vapor concentration. The frost point temperature T_f is defined as the temperature where $S = 1$. In Figure 4 we show the variation of S for a temperature deviation from a given temperature. As can be seen from this figure, S increases by a factor of 10 if the temperature drops by ~5–8 K.

[12] Since S is proportional to p_{H_2O} a water profile is needed. Unfortunately, no relevant measurements are available and we have to rely on model profiles. We have considered water vapor concentrations from the dynamical/chemical models of *Körner and Sonnemann* [2001], and from *von Zahn and Berger* [2003], respectively (in the following referred to as K&S and vZ&B, respectively). To facilitate the discussion we show the water vapor concentrations and the frost point temperatures from these models in Table 1. The vZ&B model takes into account freeze-drying but assumes stationary and quiet conditions, i.e., no mixing due to gravity waves etc. Therefore it gives rather low water vapor mixing ratios less than 0.1–0.2 ppmv above approximately 88 km. These numbers are much smaller compared to the K&S model, and also much smaller than recently published values from the HALOE satellite instrument [*McHugh et al.*, 2003]. It should be noted, however, that the northern most HALOE data are observed at 60–70°N, i.e., significantly further south compared to

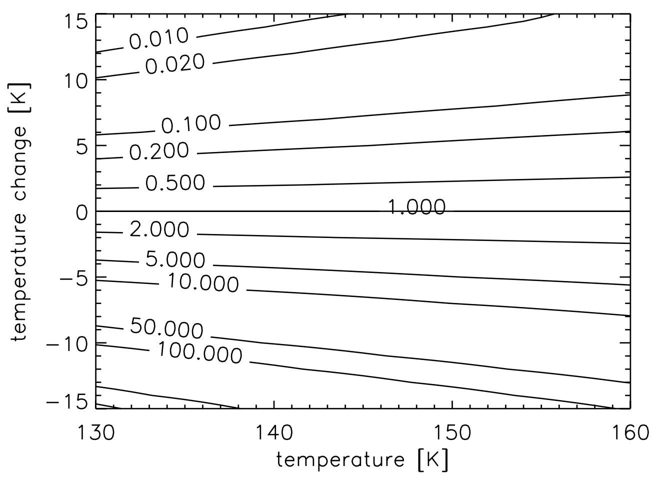

Figure 4. Relative change (factor) of the degree of saturation (S) with temperature. The isolines show the factor by which S changes if the temperatures is changed from a value given on the abscissa.

Table 1. Water Vapor Concentrations, $[H_2O]$, and Frost Point Temperatures, T_f, From the K&S and vZ&B Models, Respectively[a]

	K&S		vZ&B			
Altitude, km	$[H_2O]$, ppmv	T_f, K	$[H_2O]$, ppmv	T_f, K	Factor	Temperature Difference, K
78	5.08	154.2	4.96	154.1	1.0	0.1
79	4.95	153.4	4.81	153.3	1.0	0.1
80	4.81	152.6	4.53	152.4	1.1	0.2
81	4.62	151.8	4.00	151.3	1.2	0.5
82	4.40	151.0	3.57	150.3	1.2	0.7
83	4.12	150.0	4.48	150.3	0.9	−0.3
84	3.80	149.0	2.33	147.5	1.6	1.5
85	3.47	148.0	1.16	144.7	3.0	3.3
86	3.15	146.9	0.60	142.0	5.2	4.9
87	2.84	145.8	0.32	139.5	8.9	6.3
88	2.55	144.8	0.18	137.3	14.5	7.5
89	2.27	143.7	0.11	135.3	20.8	8.4
90	1.98	142.6	0.09	134.3	21.3	8.3
91	1.62	141.3	0.13	134.4	12.9	6.9
92	1.15	139.4	0.20	134.6	5.9	4.7
93	0.73	136.7	0.14	132.4	5.3	4.3
94	0.45	132.5	0.02	124.7	27.8	7.8

[a]See text for more details. Here "factor" refers to the ratio of water vapor concentrations, and "temperature difference" = T_f(K&S) minus T_f(vZ&B).

Spitsbergen. The vZ&B model is available for midsummer only, whereas the K&S model varies with season. We have therefore decided to primarily use H_2O values from the K&S model but we will also discuss the implications when using the vZ&B model profile.

3.3. Temperatures During PMSE

[13] In Figure 5 three temperature profiles measured by falling sphere are shown corresponding to the flights marked in Figure 1. We have also plotted the PMSE profile given by averaging for approximately ±1 h around the rocket launch. It should be noted that the horizontal distance between the actual falling sphere descent and the radar volume is on the order of 50 km which corresponds to a time shift of ~30 minutes assuming a mean line of sight wind velocity of 20–30 m/s (if one would reasonably assume that larger-scale PMSE structures are persistent over this period and are advected with the background wind). In Figure 5 we also show two frost point T_f profiles using water vapor concentrations from K&S and vZ&B. Temperatures are below T_f in an extended altitude range in all three flights. The lower edge nicely agrees with the lower edge of

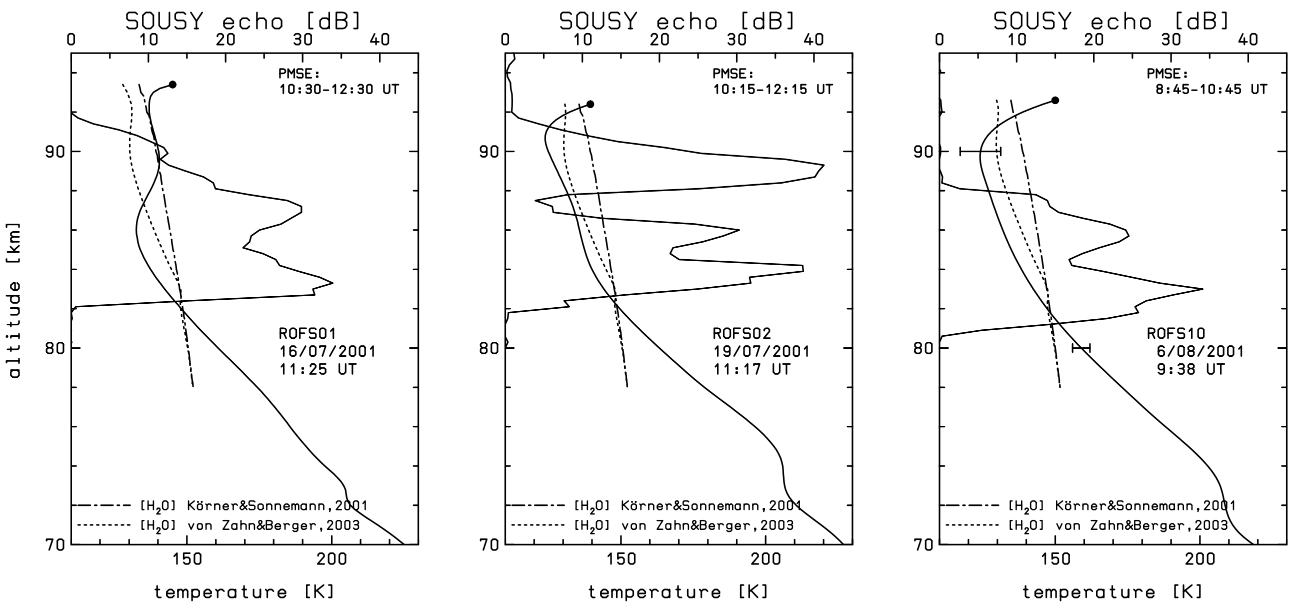

Figure 5. Temperature profiles measured for flights ROFS01, ROFS02, and ROFS10 (thick solid line). The flight labels, launch dates, and times are indicated in the inlet. In the right plot we have indicated the error bar at 90 and 80 km,. The dotted and dashed lines indicate frost point temperatures T_f using model water vapor mixing ratios from *von Zahn and Berger* [2003] and from *Körner and Sonnemann* [2001], respectively. The thin solid line presents the PMSE echo (upper abscissa) averaged for approximately ±1 hour around the rocket launch.

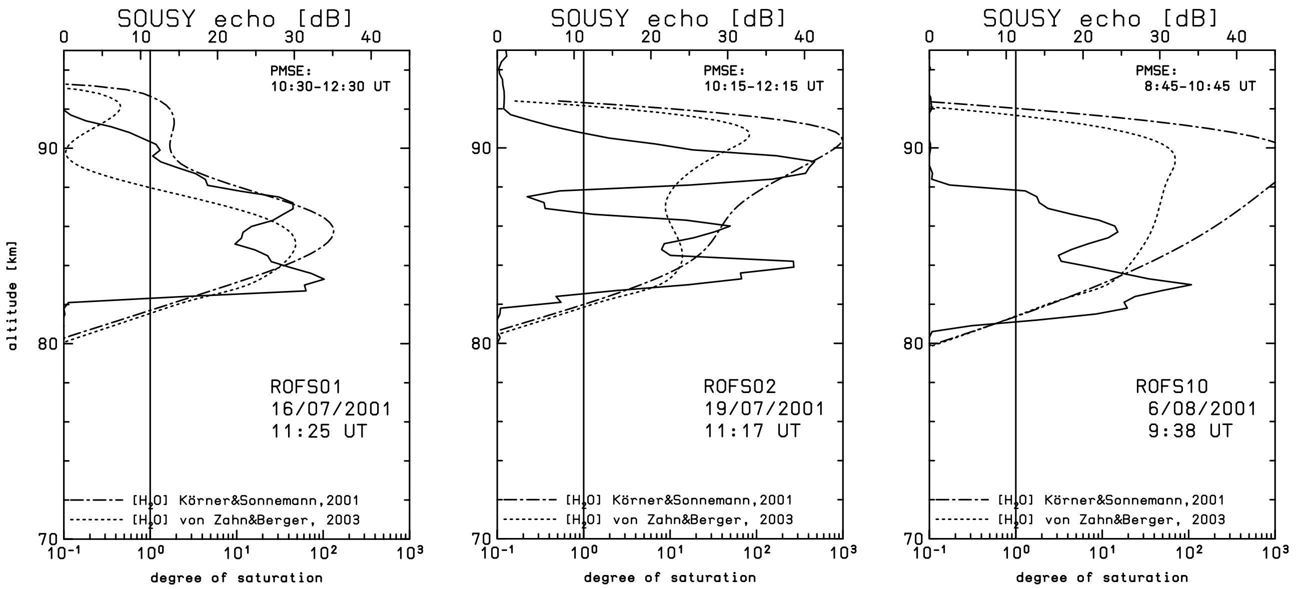

Figure 6. Same as Figure 5 but for the degree of saturation, S. The dotted and dashed lines indicate S profiles using model water vapor mixing ratios from *von Zahn and Berger* [2003] and from *Körner and Sonnemann* [2001], respectively. The solid line presents the PMSE echo (upper abscissa) averaged for approximately ±1 hour around the rocket launch.

PMSE but the upper edge sometimes agrees (ROFS01 and ROFS02) and sometimes does not (ROFS10). This result is even more evident when studying the corresponding height profiles of S which are shown in Figure 6. There is general agreement between the altitude ranges of S > 1 and PMSE, but there are also deviations, in particular in the upper part of the PMSE (see, for example, flight ROFS10). For ROFS01 and ROFS02 there is close correspondence between the shape of the PMSE and the S profiles. We will later discuss the correlation between radar signal strength (which is a measure of the scatter cross section of the PMSE irregularities) and the degree of saturation. It is interesting to note that the double layered PMSE structure observed during ROFS02 can also be seen in the S profile although the maxima do not coincide exactly.

[14] A comparison of S profiles derived from FS temperatures and PMSE is shown in Figure 7. We concentrate on flights up to ROFS17 launched on 23 August which covers the main PMSE season. Again, the PMSE profiles shown are derived by averaging of ~±1 h around the rocket launch. This smears out double layer structures as observed, e.g., in Figure 1. We have marked the height range of 0.3 < S < 1 to indicate the potential uncertainty in S discussed in section 3.2. The S values at the edges of the PMSE layer are noted in the plot. PMSE occur nearly exclusively at altitudes where S > 1, but the reverse is not true (see for example flights ROFS03, ROFS06, and ROFS10). This result is made clearer in Figure 8 where the temperatures within and outside the PMSE layers are compared to the frost point temperature T_f. Within PMSE layers temperatures are nearly always smaller than T_f. In the lower part of Figure 8 we have plotted temperatures at altitudes with the proven absence of PMSE. Outside the main PMSE height range both cases occur ($T > T_f$ and $T < T_f$) which demonstrates that a low enough temperature is a necessary but not sufficient condition for PMSE at these altitudes. We will later discuss the potential explanation for this observation.

[15] In Figure 9 we summarize the results on supersaturation and its comparison with PMSE again for flights up to and including ROFS17. In the main height range of PMSE (approximately 83–88 km) PMSE are present during all flights and there are basically no cases with S > 1 and no PMSE, i.e., every time that it is cold enough for ice particles to exist at these altitudes, PMSE are present, and vice versa. Below and above the main PMSE layer there are a few flights when PMSE is present but the supersaturation condition is not fulfilled, i.e., S is smaller than 1. All these cases disappear, however, if we allow for an error in S of a factor of 3 which corresponds to −(2–3) K or correspondingly lower water vapor mixing ratios. These uncertainties are well within our experimental and model uncertainties. Keeping this limitation in mind we conclude that PMSE exclusively occur when it is cold enough for ice particles to exist. Above ~87 km we frequently find height ranges with S > 1 but no PMSE (see also Figure 7). We will discuss these observations in section 4.1.

3.4. Noctilucent Clouds

[16] Details of the NLC measurements during the ROMA campaign are presented in the work of *Höffner et al.* [2003]. NLCs were observed from 12 June (the first day of operation) until 12 August when a period of bad weather started. When the lidar was switched on again on 26 August, no NLC was observed. The mean occurrence frequency in the period 12 June to 12 August is 77%. The mean of all individual NLC peak altitudes is 83.6 km and does not show a significant variation with season. The average top and bottom altitude of the NLC layer is 85.1 and 82.5 km, respectively [*Höffner et al.*, 2003]. We have also determined statistical properties from the combined data set 2001 and 2003 and found very similar values (occurrence frequency: 74%; mean

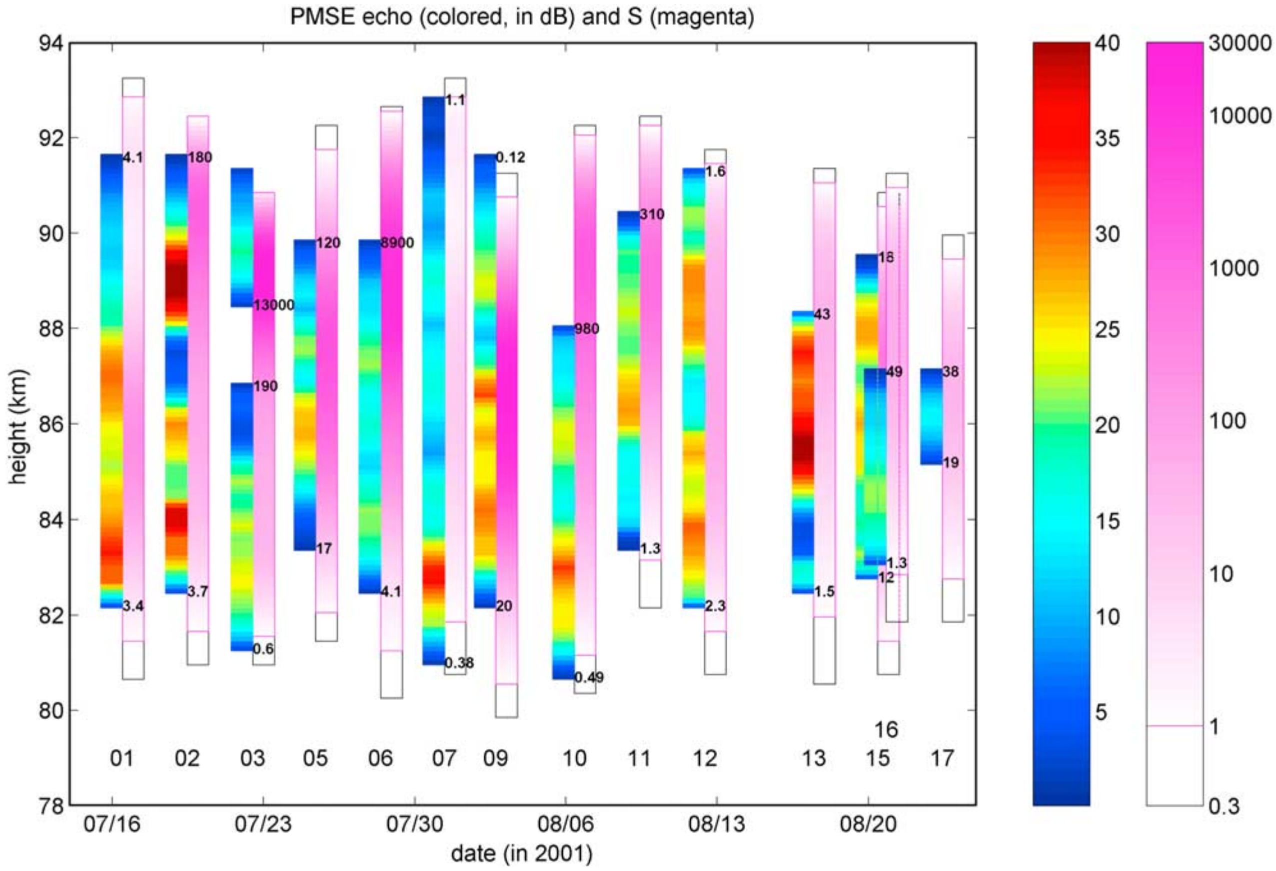

Figure 7. Comparison of all individual S profiles derived from FS measurements and PMSE averaged for ±1 hour around the rocket flight. The numbers below the bars give the FS flight numbers. The radar echo above noise is shown in dB, color-coded from blue to red. The S values are shown in pink from 0.3 to 30,000. The numbers in the pink columns give the S values at the edges of the PMSE layers. There are no temperatures available at the top of the PMSE layer during ROFS03.

peak altitude: 83.5 km) which demonstrates that the conditions during the ROMA campaign are representative. In Figure 10 we show all NLC observed during the ROMA campaign as a function of season and altitude together with the S = 1 line derived from the FS temperature climatology and the K&S water vapor profiles. It is obvious from this figure that NLC exist only in the lower part of the height range with S > 1. We will discuss this observation in more detail later. There is no obvious correlation between the magnitude of S and the signal strength, more precisely the backscatter coefficient, BSC (for a detailed explanation of BSC, see *Höffner et al.* [2003]).

4. Discussion

[17] In this section we discuss the potential geophysical implications of the observations presented above, in particular the relationship of PMSE and ice particles. We will make use of the understanding of PMSE as presented in the work of *Rapp and Lübken* [2003], in particular regarding the influence of ice particles on the lifetime of plasma fluctuations at meter scales.

4.1. Individual Profiles

[18] From the comparison of individual temperature profiles and PMSE we have seen that there is general agreement between the height ranges of S > 1 and PMSE. In the majority of the cases S is largest in the center of the PMSE layer (∼84–88 km) and has typical values of 10–100. This implies that actual temperatures are smaller than the frost point temperatures by approximately 5–10 Kelvin.

[19] Occasionally, S can be larger than 1 by a factor of up to 13000 in the mesopause region but no PMSE exists (see, e.g., flights ROFS03 and ROFS10 in Figure 7). The S values at the PMSE edges are systematically larger in the upper part of PMSE (above 85 km) compared to the lower part (see Figure 7). The corresponding mean values are 1600 and 6 but with a rather large variability. How can S be so large above ∼85 km but no PMSE exists? There are various potential explanations for this observation (see below) but it seems likely that the actual water vapor mixing ratio is significantly smaller compared to the K&S model in line with the freeze-drying effect. Indeed, model calculations by vZ&B give [H_2O] ∼ 0.18 ppmv at 88 km (or smaller, depending on model conditions) whereas the K&S gives ∼2.5 ppmv, i.e., 1–2 orders of magnitude larger (see Table 1). We realize that PMSE require a minimum ice particle radius of ∼3 nm to significantly affect the plasma. However, for K&S water vapor concentrations it takes only 2–3 h and a very small height range (100–200 m) for particles to grow to this size. A typical time constant for the persistence of PMSE is much larger.

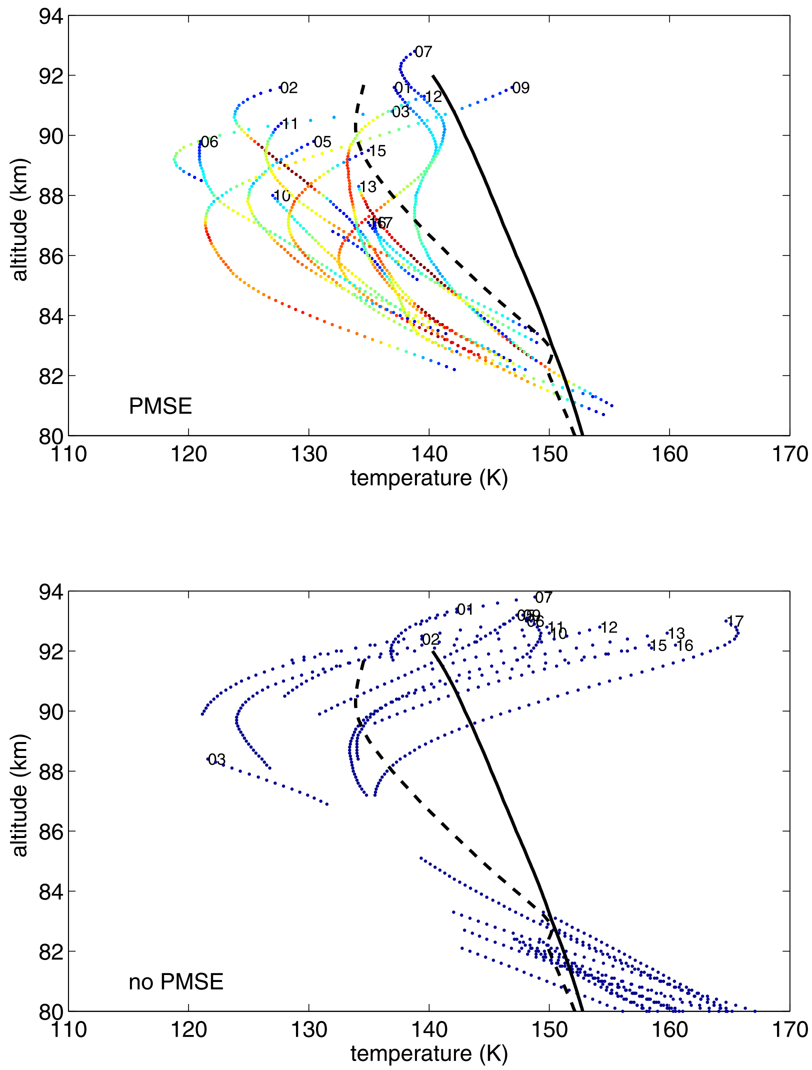

Figure 8. (top) Temperatures in the PMSE layer and (bottom) in the proven absence of PMSE. The numbers in the plot give the FS flight numbers. The solid and dashed lines show the frost point temperature profiles using [H_2O] values from the K&S and vZ&B models, respectively. The colors in the temperature profiles indicate the radar echo power in dB (color code from Figure 7).

For example, the PMSE during flight ROFS10 was very similar for many hours before and after the period shown in the lower panel of Figure 1. An alternative explanation would be that our temperatures are systematically too low by up to 15–25 Kelvin which is rather unlikely since these deviations are considerably larger than the instrumental uncertainty. A comparison with more sophisticated high resolution temperature measurements has shown that the mean thermal structure around the mesopause is nicely reproduced by the falling sphere technique [*Rapp et al.*, 2002b]. Of course, temperatures around the mesopause are presumably variable in time and could have been significantly higher immediately prior to the rocket launch. Again, this is rather unlikely since we observe large S values in nearly all flights which argues against a very specific scenario. Why should the temperatures have been systematically larger prior to the rocket launches? Although unlikely, we cannot rule out this possibility from our observations.

[20] Could it be that neutral turbulence is missing which is initially required to create PMSE? Again, this explanation is unlikely since (as will be shown later) turbulence is obviously frequent enough to not significantly influence the seasonal and height distribution of PMSE. Furthermore, in situ turbulence measurements at 69°N show maximum turbulence occurrence rates around 90 km [*Lübken et al.*, 2002] and the potential explanation for this result (breaking of gravity waves) is also valid at higher latitudes. A necessary condition for the existence of PMSE is a sufficient number of free electrons. *Rapp et al.* [2002a] has shown that PMSE can occur for electron number densities in excess of $\sim$300–500/cm^3. The International Reference Ionosphere shows that this condition is fulfilled permanently at 78°N at PMSE altitudes from mid-April to end of August due to ionisation by solar Ly$_\alpha$ radiation. We summarize that most likely the actual water vapor mixing ratio around the mesopause is much smaller than the K&S values in line with the freeze-drying scenario of vZ&B.

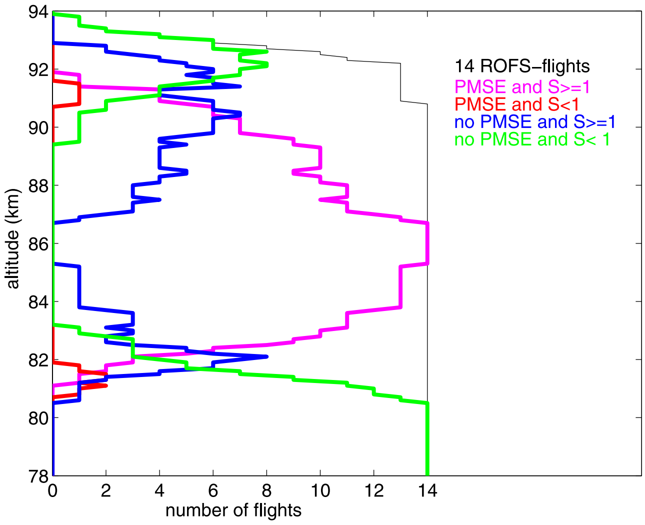

Figure 9. Number of flights with/without PMSE and with/without S = 1 as a function of altitude. Flights up to ROFS17 are considered in this statistics which covers the main PMSE season (the total number of FS flights is 14 since there were also some chaff flights). Four different cases are shown: (1) simultaneous occurrence of PMSE and supersaturation ($S \geq 1$, red); (2) PMSE and no supersaturation ($S < 1$, pink); (3) no PMSE and supersaturation ($S \geq 1$, blue), and (4) no PMSE and no supersaturation (green).

We note that microphysical modeling of ice particle growth in the summer mesopause region with and without gravity waves also show a water vapor reduction around the mesopause [*Rapp et al.*, 2002b].

[21] We have found no correlation between PMSE power and the degree of saturation or temperature. We explain this observation by the fact that the size of the ice particles is not solely determined by local temperatures and water vapor concentrations but also by the history of the nucleation and by the variability of the background field etc. [*Berger and von Zahn*, 2002; *Rapp et al.*, 2002b]. Still, it must be cold enough for ice particles to exist for reducing the electron diffusivity but this condition does not determine the size of the ice particles.

4.2. Climatology

[22] In a climatological sense the variation of PMSE with altitude and season is entirely determined by the thermal structure as can be seen by comparing the S = 1 lines in the lower panel of Figure 2 with the occurrence of PMSE. We have drawn the S = 1 line using water vapor mixing ratios from K&S and have varied temperatures by ±5 K. We have also plotted the S = 1 line with [H_2O] from the vZ&B model but only for the main summer season (up to mid-August) since this model is valid for midsummer only whereas the background conditions (temperatures, horizontal and vertical winds etc.) start to deviate from midsummer conditions after mid-August. The S = 1 line from vZ&B is practically identical to K&S at the lower PMSE edge and is somewhat lower in altitude at the upper edge. The latter is caused by lower water vapor concentrations in this model (freeze-drying) which require lower temperatures for S = 1. Since the upper edges of PMSE are found above the mean mesopause height, lower temperatures are found at lower altitudes.

[23] We now compare the S = 1 lines from both models with the seasonal variation of the upper edge of PMSE. We should keep in mind that the models and the observations represent different temporal and spatial scales: the models represent mean conditions (no variability) whereas the PMSE varies from day to day (and even on shorter timescales) since the conditions for PMSE vary with time and space (temperatures, water vapor, turbulence, transport etc.). Furthermore, we have to take into account the uncertainties in the measurements and in the models (see section 3.2). Considering the different temporal and spatial scales and the

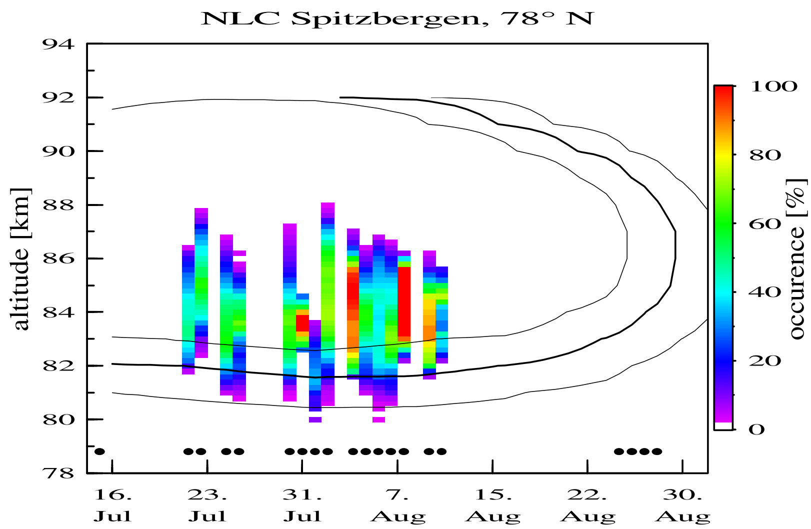

Figure 10. NLC observed by the K lidar during the ROMA campaign in 2001 and the S = 1 line using the FS temperature climatology and water vapor mixing ratios from K&S. Temperatures have been varied by ±5 K (thin lines). Days where measurements were made are marked by a dot above the lower abscissa.

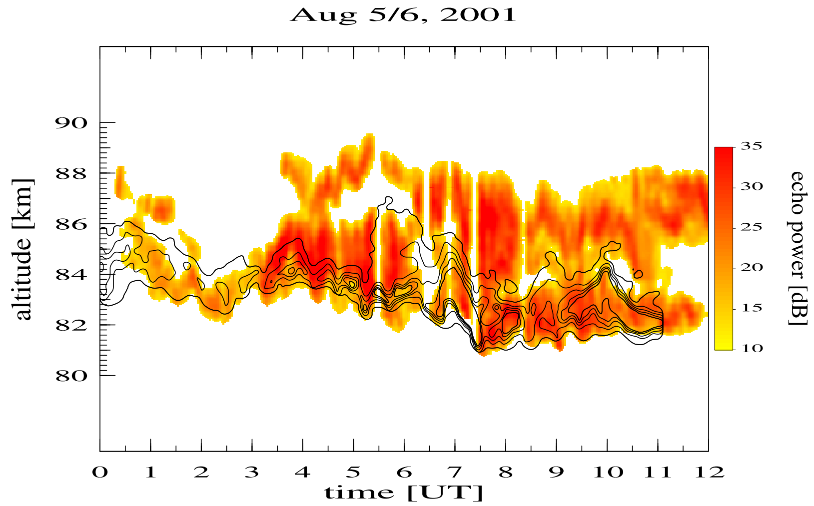

Figure 11. Common measurement of PMSE and NLC on 5/6 August 2001 at Spitsbergen. The radar echo power above noise is shown in dB (color contour). The backscatter ratios measured by the K lidar are shown in the (unlabeled) black contour lines.

uncertainties we cannot decide which model is correct which implies that we can not detect the freeze-drying effect by comparing the S = 1 lines with the seasonal variation of PMSE but only in specific cases (as demonstrated above).

[24] The fact that the S = 1 lines in the lower panel of Figure 2 nicely contours the PMSE variation implies that small-scale structures in the plasma are present frequently enough to not significantly influence the seasonal and height variation of PMSE. This also means that neutral air turbulence in combination with slow decay times of plasma irregularities are present sufficiently frequently. We will come to a more quantitative analysis shortly.

[25] Can we identify a reason for the markedly reduction of PMSE around 15 August? There is no instrumental explanation for this effect, i.e., the radar performance was nominal in this period. A falling sphere was launched on 17 August (ROFS13) and showed no apparent deviation of the temperature profile from the climatological mean. However, the occurrence decrease had almost recovered when ROFS13 was flown. We conclude that there is no apparent explanation for the reduced PMSE activity. It could have been caused by extraordinary conditions in water vapor concentrations, turbulence, and/or plasma parameters. Considering the small temperature variability it seems unlikely that high temperatures have caused this decrease but this possibility cannot be ruled out from our observations.

[26] As can be seen in Figure 3 the PMSE occurrence rate is largest around ~85 km, whereas S is largest around 88 and 86 km for the K&S and vZ&B models, respectively. It is tempting to explain the better agreement between the PMSE distribution and the vZ&B line with freeze effect in this model. It is not clear, however, how PMSE occurrence rates are related to S (we have seen already that PMSE power(!) does not correlate with S). More insight comes from microphysical modeling of ice particle nucleation and charging resulting in maximum values of $|Z_A|N_A \times r_A^2$ (Z_A is the particle charge; see *Rapp et al.* [2002b, Figure 7] and *Rapp et al.* [2003, Figures 4 and 9]). As can be seen from these model calculations the maximum concentration of "many" charged ice particles with sufficiently large radii is not necessarily colocated with the height of largest S values but is given by a complicated interaction of particle nucleation and growth when the particles move through (and modify) the background atmosphere. Certainly, the temperature structure of the upper mesosphere/lower thermosphere is the most important ingredient in this model calculations. Future modeling is required to better understand the dependence of PMSE occurrence frequency on the mean state and the variability of background temperatures and water vapor.

[27] We note that the main features of PMSE during the ROMA campaign are very similar to those observed in previous years [*Rüster et al.*, 2001]. This indicates that the main conclusions drawn from our comparison of temperatures, NLC, and PMSE are representative for northern polar cap latitudes in general.

4.3. NLC, PMSE, and Temperatures

[28] An example of simultaneous PMSE and NLC measurements is shown in Figure 11. The close correlation between both phenomena is obvious. The NLC covers the lower part of the PMSE which is very typical and has been observed before at lower latitudes [*Nussbaumer et al.*, 1996; *von Zahn and Bremer*, 1999]. The mean variation of NLC appearance with height and season is in agreement with the climatological variation of supersaturation derived from the FS temperature measurements [see *Lübken and Müllemann*, 2003, Figure 4]. This is true even if we consider the uncertainty of S caused by the unknown water vapor concentration discussed in section 3.2. At the end of the lidar NLC period (12 August, i.e., when measurements had to be terminated due to bad weather) temperatures are still low enough for supersaturation. When the lidar was started again on 26 August temperatures had just become too high for supersaturation and indeed no NLC was observed. This highlights the very close correspondence of NLC and the thermal structure. The differences between NLC and PMSE occurrence frequencies (77% versus 100%) and height

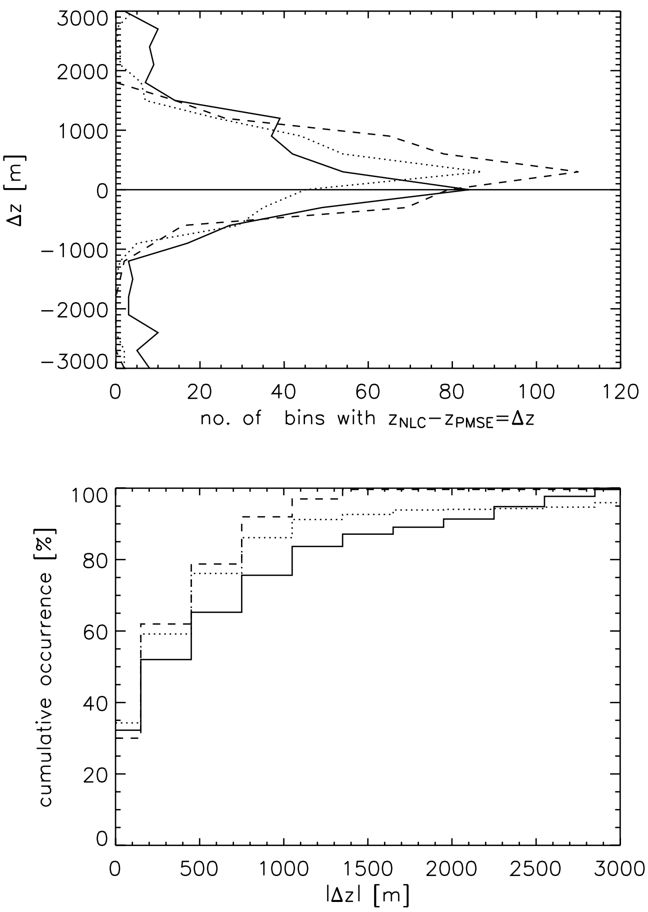

Figure 12. Summary of altitude differences of the lower edges of NLC and PMSE ($z_{NLC} - z_{PMSE}$) for the three best common measurements in 2001: 25/26 July (solid line), 30/31 July (dotted line), and 5/6 August (dashed line). The corresponding mean altitudes are 280, 510, and 300 m. (top) Number of bins given by a time slot of 2 min. (bottom) Cumulative number of cases in percent as a function of the magnitude of the altitude difference.

distribution are caused by the different sensitivities to particle size. Whereas PMSE are observed nearly as soon as particles are present, NLC require a minimum size of approximately 20 nm.

[29] There is nearly perfect agreement of the lower edges of NLC and PMSE even when the height of this edge varies by several kilometers throughout the 12 hours shown in Figure 11. We have summarized the altitude differences for three nights with the best available time series in Figure 12. The mean of the altitude difference is ~300–500 m and ~80% of all differences are within a range of ±600 m around zero. These numbers should be compared with the combined altitude resolution of the lidar (200 m) and the radar (300 m). We note that we are comparing absolute altitude determinations from two independent instruments. This means that the differences stated above include all potential errors caused by signal propagation uncertainties in the electronics of the lidar and radar, height calibration of the radar (careful checks showed that the estimated error is about 100 m), etc. The fact that the differences are very small indicate that these instrumental errors are small.

[30] Combining the equations for the growth rate and the fall velocity of ice particles determines the rate of change of aerosol radius with height [*Gadsden*, 1981]. Using the temperature profile from the Spitsbergen climatology we find the S = 1 level and the largest size ice particles at 83.6 km at a temperature of 143 K. Below that altitude particles melt and shrink. If we take $r_A = 20$ and $r_A = 3$ nm as an approximate detection limit for NLC and PMSE, respectively, we find these particle sizes at heights of 82.76 and 82.59 km, i.e., separated by less then 200 m, in nice agreement with our observations. Our simple model results are supported by more sophisticated calculations by the COMMA/IAP model (Cologne Model of the Middle Atmosphere/Institute of Atmospheric Physics Kühlungsborn) which takes into account particle size distributions, latitude variation of temperatures, horizontal and vertical winds, etc. This model also gives typical NLC/PMSE lower height differences of ~200 m (U. Berger, private communication, 2003). We have varied the temperature gradient dT/dz below the S = 1 level and found that the altitude difference between the lower edge of NLC and PMSE is very insensitive against variations in dT/dz, provided that temperatures stay warm enough so that ice particles evaporate.

[31] The close match between the lower edges of NLC and PMSE is even more remarkable if we consider the very different field of view of the lidar and radar, respectively. The K laser beam width is 200 μrad which corresponds to a diameter of ~20 m at 85 km. The radar half power beam width is 4° which corresponds to a diameter of ~6000 m at 85 km. Our observations imply that these layers are horizontally homogeneous (within less than few hundred meters) at scales of at least several kilometers. The results stated above are for the vertical beam of the radar which has a horizontal distance of approximately 10 km from the lidar beam. We have repeated the analysis for one of the oblique beams of the radar which is very close to the lidar beam and did not find any significant difference to the vertical beam. This again confirms the horizontal homogeneity of the ice clouds.

[32] As can be seen in Figures 11 and 12 there are also cases when the NLC appears below the PMSE (though within a very short distance) which are not covered by the explanation given above. These cases are presumably due to small horizontal homogeneities (see above). We cannot rule out that the electron concentration is too low at these altitudes to make PMSE. However, this is unlikely due to ionization by Ly_α which is present practically permanently at this high latitude in summer and penetrates down to ~75 km.

[33] The height differences between the upper edge of NLC and PMSE are significantly larger than at the lower edges which is explained by the comparatively long time (and height) it takes for particles to grow from 3 nm to 20 nm, whereas evaporation occurs much faster. A detailed comparison of these observations with model studies will presumably constrain the various scenarios on particle nucleation, growth, sedimentation, and evaporation.

4.4. PMSE and Turbulence

[34] The fact that PMSE at Spitsbergen occur practically permanently has important consequences for the occurrence rate of turbulence. After all, small-scale plasma irregulari-

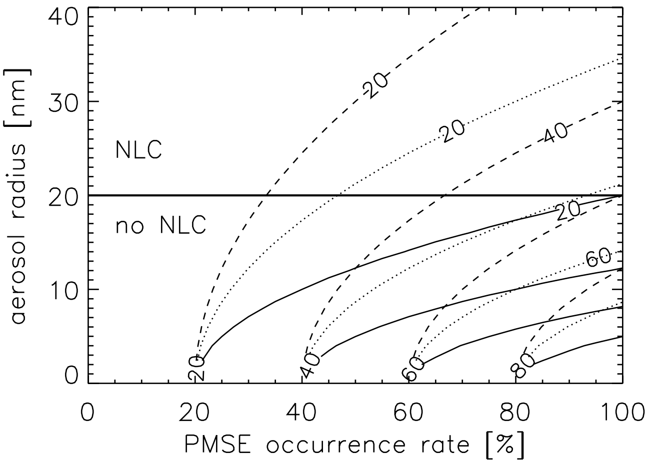

Figure 13. Turbulence occurrence rate as a function of PMSE occurrence rate and aerosol particle radius. Three different turbulence life times have been assumed: 10 min (solid line), 30 min (dotted line), and 60 min (dashed line). The horizontal line shows the approximate size limit for ice particles to be seen as NLC.

ties initially caused by neutral air turbulence are most likely the prime physical quantity causing the strong radar echoes. The reduction of the electron diffusivity, D, causes these plasma fluctuations to extend beyond the smallest scales in the neutral turbulence field. This implies that the Schmidt number, Sc = ν/D (ν = kinematic viscosity of air) is significantly larger than 1. From theory we know that plasma fluctuations can persist after neutral air turbulence has stopped due to the slow decay time of aerosol irregularities. The decay time τ is proportional to r_A^2 (r_A = aerosol radius) and we find $\tau \sim 0.1 \cdot r_A^2$ (τ in minutes and r_A in nm) [*Rapp and Lübken*, 2003]. Let us assume that neutral air turbulence is present for a time T_{turb} and that the Schmidt number is large enough to produce plasma fluctuations at the radar half wavelength. Then the duration of PMSE is $T_{turb} + \tau$. The occurrence rates of PMSE, O_{PMSE}, and neutral turbulence, O_{turb}, are related as

$$O_{turb} = O_{PMSE} \cdot \frac{T_{turb}}{T_{turb} + \tau}. \quad (1)$$

[35] In Figure 13 we have plotted turbulence occurrence rates as a function of PMSE occurrence rates and r_A for various T_{turb}. For very small aerosol radii, τ is very small and $O_{turb} \approx O_{PMSE}$. For large radii, τ is large and $O_{turb} \propto O_{PMSE}/r_A^2$. If no NLC are present particles must be smaller than approximately 20 nm which limits the range of r_A. With $O_{PMSE} \sim 100\%$ (as observed) and $r_A < 20$ nm we see that turbulence occurrence rates are restricted to 20–100%, probably closer to the larger limit since particles are presumably as small as 5–10 nm within PMSE. The case that NLC occur but no PMSE is very rare and does not significantly influence the estimates from above.

5. Summary

[36] In summary, PMSE (NLC) appear in the entire (lower) part of the height range of supersaturation but details of their morphology, such as short term variability, signal strength (radar reflectivity or scatter cross section), BSC, layer width etc., do not depend solely on the local thermal structure. If PMSE are present temperatures are smaller than T_f, i.e., it is cold enough for ice particles to exist. This puts major constraints on model calculations of the thermal and chemical state of the polar summer mesosphere and also allows for a simple test of temperature measurements.

[37] We have seen that the systematic differences between regions of supersaturation and PMSE indicates lower H_2O values in the upper part of the PMSE layer (above approximately 85 km) compared to the K&S model. This is in line with the freeze-drying effect transporting water vapor from the mesopause region to approximately 82–83 km where ice particles melt. On the other hand, the mean variation of PMSE and NLC appearance with height and season is in nice agreement with the climatological variation of the thermal structure in the upper mesosphere. We have not found a correlation between PMSE power and the degree of saturation which indicates that (amongst other ingredients required for PMSE) the size of the ice particles is not solely determined by local conditions (temperatures and water vapor) but also by the history of the nucleation and by the variability of the background field etc. Regarding NLC, we should keep in mind that it can take several hours before an ice particle reaches a size detectable by lidar [*Berger and von Zahn*, 2002; *Rapp et al.*, 2002b]. During this time the particle is carried hundreds of kilometers by the mean wind and the background conditions relevant for ice particle formation have most likely varied.

[38] Comparison of NLC, PMSE and T(z) supports the standard scenario: ice particles start to nucleate around the mesopause. Here, they are too small to be seen by lidar but affect the plasma thereby creating PMSE. Ice particles fall and grow in size until they are large enough to be seen by lidar ($r_A > 20$ nm). They fall further down and disappear quickly since temperature rises rapidly with altitude. The quantitative results on the height distance between the upper (and lower) edges of NLC and PMSE constrain the various scenarios on particle nucleation, growth, sedimentation, and evaporation.

[39] The now available better understanding of PMSE allows to draw important conclusions about the occurrence frequency of neutral air turbulence from the statistics of PMSE observed at Spitsbergen. We have seen that the seasonal and height variation of PMSE is determined by the thermal structure which implies that turbulence must be present rather frequently at 78°N. Future model calculations of the thermal and dynamical status of the upper atmosphere at very high polar latitudes will have to take these results into consideration.

[40] **Acknowledgments.** The SOUSY radar data were collected in close cooperation with the Max-Planck-Institut für Aeronomie in Katlenburg-Lindau. We thank Jenn-Shyong Chen, and Jörg Trautner for their assistance in operating the radar and analysing the data. The support for the lidar measurements during ROMA in Spitsbergen by Cord Fricke-Begemann, Jens Lautenbach, Peter Menzel, Jian Liu, and Peter Keller is kindly appreciated. The ROMA rocket campaign was conducted with the excellent support of the crew of the Mobile Raketenbasis (DLR, Germany) and the Andøya Rocket Range. Arno Müllemann has kindly performed the data analysis for the falling spheres. We thank Uwe Berger for his model calculations on the altitude difference between NLC and PMSE and Markus

Rapp for stimulating discussions. This project was supported by the Bundesministerium für Bildung, Wissenschaft, Forschung und Technologie, Bonn, under grants 50 OE 99 01 (ROMA) and AFO 07 ATF 41 (OPOSSUM).

References

Berger, U., and U. von Zahn (2002), Icy particles in the summer mesopause region: Three-dimensional modeling of their environment and two-dimensional modeling of their transport, *J. Geophys. Res.*, *107*(A11), 1366, doi:10.1029/2001JA000316.

Blix, T. A., M. Rapp, and F. J. Lübken (2003), Relations between small-scale electron number density fluctuations, radar backscatter, and charged aerosol particles, *J. Geophys. Res.*, *108*(D8), 8450, doi:10.1029/2002JD002430.

Cho, J. Y. N., and J. Röttger (1997), An updated review of polar mesosphere summer echoes: Observation, theory, and their relationship to noctilucent clouds and subvisible aerosols, *J. Geophys. Res.*, *102*, 2001–2020.

Cho, J. Y. N., T. M. Hall, and M. C. Kelley (1992), On the role of charged aerosols in polar mesosphere summer echoes, *J. Geophys. Res.*, *97*, 875–886.

Czechowsky, P., J. Klostermeyer, J. Röttger, R. Rüster, and G. Schmidt (1998), The SOUSY-Svalbard-Radar for middle and lower atmosphere research in the polar region, in *Proceedings of the 8th Workshop on Technical and Scientific Aspects of MST Radar*, edited by B. Edwards, pp. 318–321, SCOSTEP, Boulder, Colo.

Fiedler, J., G. Baumgarten, and G. von Cossart (2003), Noctilucent clouds above ALOMAR between 1997 and 2001: Occurrence and properties, *J. Geophys. Res.*, *108*(D8), 8453, doi:10.1029/2002JD002419.

Fricke-Begemann, C., M. Alpers, and J. Höffner (2002), Daylight rejection with a new receiver for potassium resonance temperature lidars, *Opt. Lett.*, *27*(21), 1932–1934.

Gadsden, M. (1981), The silver-blue cloudlets again: Nucleation and growth of ice in the mesosphere, *Planet. Space Sci.*, *29*, 1079–1087.

Gadsden, M., and W. Schröder (1989), *Noctilucent Clouds*, Springer-Verlag, New York.

Hansen, G., M. Serwazi, and U. von Zahn (1989), First detection of a noctilucent cloud by lidar, *Geophys. Res. Lett.*, *16*, 1445–1448.

Hill, R. J., D. E. Gibson-Wilde, J. A. Werne, and D. C. Fritts (1999), Turbulence-induced fluctuations in ionization and application to PMSE, *Earth Planet Space*, *51*, 499–513.

Höffner, J., C. Fricke-Begemann, and F.-J. Lübken (2003), First observarions of noctilucent clouds by lidar at Svalbard, 78°N, *Atmos. Chem. Phys.*, *3*, 1101–1111.

Kelley, M. C., D. T. Farley, and J. Röttger (1987), The effect of cluster ions on anomalous VHF backscatter from the summer polar mesosphere, *Geophys. Res. Lett.*, *14*, 1031–1034.

Körner, U., and G. R. Sonnemann (2001), Global three-dimensional modeling of the water vapor concentration of the mesosphere-mesopause region and implications with respect to the noctilucent cloud region, *J. Geophys. Res.*, *106*, 9639–9651.

Lie-Svendson, Ø., T. A. Blix, U.-P. Hoppe, and E. V. Thrane (2003), Modeling the plasma response to small-scale aerosol particle perturbations in the mesopause region, *J. Geophys. Res.*, *108*(D8), 8442, doi:10.1029/2002JD002753.

Lübken, F.-J., and A. Müllemann (2003), First in situ temperature measurements in the summer mesosphere at very high latitudes (78°N), *J. Geophys. Res.*, *108*(D8), 8448, doi:10.1029/2002JD002414.

Lübken, F.-J., G. Lehmacher, T. Blix, U.-P. Hoppe, E. Thrane, J. Cho, and W. Swartz (1993), First in-situ observations of neutral and plasma density fluctuations within a PMSE layer, *Geophys. Res. Lett.*, *20*, 2311–2314.

Lübken, F.-J., M. Rapp, and P. Hoffmann (2002), Neutral air turbulence and temperatures in the vicinity of polar mesosphere summer echoes, *J. Geophys. Res.*, *107*(D15), 4273, doi:10.1029/2001JD000915.

Mauersberger, K., and D. Krankowsky (2003), Vapor pressure above ice at temperatures below 170 K, *Geophys. Res. Lett.*, *30*(3), 1121, doi:10.1029/2002GL016183.

McHugh, M., M. Hervig, B. Magill, R. E. Thompson, E. Remsberg, J. Wrotny, and J. Russell III (2003), Improved mesospheric temperature, water vapor and polar mesospheric cloud extinctions from HALOE, *Geophys. Res. Lett.*, *30*(8), 1440, doi:10.1029/2002GL016859.

Nussbaumer, V., K.-H. Fricke, M. Langer, W. Singer, and U. von Zahn (1996), First simultaneous and common-volume observations of NLC and PMSE by lidar and radar, *J. Geophys. Res.*, *101*, 19,161–19,167.

Rapp, M., and F.-J. Lübken (2003), On the nature of PMSE: Electron diffusion in the vicinity of charged particles revisited, *J. Geophys. Res.*, *108*(D8), 8437, doi:10.1029/2002JD002857.

Rapp, M., J. Gumbel, F.-J. Lübken, and R. Latteck (2002a), D region electron number density limits for the existence of polar mesosphere summer echoes, *J. Geophys. Res.*, *107*(D19), 4187, doi:10.1029/2001JD001323.

Rapp, M., F.-J. Lübken, A. Müllemann, G. Thomas, and E. Jensen (2002b), Small-scale temperature variations in the vicinity of NLC: Experimental and model results, *J. Geophys. Res.*, *107*(D19), 4392, doi:10.1029/2001JD001241.

Rapp, M., F.-J. Lübken, P. Hoffmann, R. Latteck, G. Baumgarten, and T. Blix (2003), PMSE dependence on aerosol charge number density and aerosol size, *J. Geophys. Res.*, *108*(D8), 8441, doi:10.1029/2002JD002650.

Röttger, J. (1994), Polar mesosphere summer echoes: Dynamics and aeronomy of the mesosphere, *Adv. Space Res.*, *14*(9), 123–137.

Röttger, J. (2001), Observations of the polar D-region and the mesosphere with the EISCAT Svalbard Radar and the SOUSY Svalbard Radar, *Mem. Natl. Inst. Polar Res.*, *54*, 9–20.

Rüster, R., J. Röttger, G. Schmidt, P. Czechowsky, and J. Klostermeyer (2001), Observations of mesospheric summer echos at VHF in the polar cap region, *Geophys. Res. Lett.*, *28*, 1471–1474.

Schmidlin, F. J. (1991), The inflatable sphere: A technique for the accurate measurement of middle atmosphere temperatures, *J. Geophys. Res.*, *96*, 22,673–22,682.

Thayer, J. P., M. Rapp, A. J. Gerrard, E. Gudmundsson, and T. J. Kane (2003), Gravity-wave influences on Arctic mesospheric clouds as determined by a Rayleigh lidar at Sondrestrom, Greenland, *J. Geophys. Res.*, *108*(D8), 8449, doi:10.1029/2002JD002363.

von Cossart, G., J. Fiedler, and U. von Zahn (1999), Size distributions of NLC particles as determined from 3-color observations of NLC by ground-based lidar, *Geophys. Res. Lett.*, *26*, 1513–1516.

von Zahn, U., and U. Berger (2003), Persistent ice cloud in the midsummer upper mesosphere at high latitudes: Three-dimensional modeling and cloud interactions with ambient water vapor, *J. Geophys. Res.*, *108*(D8), 8451, doi:10.1029/2002JD002409.

von Zahn, U., and J. Bremer (1999), Simultaneous and common-volume observations of noctilucent clouds and polar mesosphere summer echoes, *Geophys. Res. Lett.*, *26*, 1521–1524.

von Zahn, U., and J. Höffner (1996), Mesopause temperature profiling by potassium lidar, *Geophys. Res. Lett.*, *23*, 141–144.

J. Höffner, F.-J. Lübken, and M. Zecha, Leibniz-Institut für Atmosphärenphysik, Schloss-Str. 6, D-18225 Kühlungsborn, Germany. (luebken@iap-kborn.de)

J. Röttger, Max-Planck-Institut für Aeronomie, Max-Planck-Str. 2, D-37191 Katlenburg-Lindau, Germany.